HHS Public Access

Author manuscript

Ocul Surf. Author manuscript; available in PMC 2023 July 03.

Published in final edited form as:

Ocul Surf. 2022 October ; 26: 300–309. doi:10.1016/j.jtos.2021.11.005.

Spontaneous acinar and ductal regrowth after meibomian gland atrophy induced by deletion of FGFR2 in a mouse model

Xiaowei Yang[a], **Xingwu Zhong**[a,b,*], **Andrew JW. Huang**[c], **Lixing W. Reneker**[d]

[a]State Key Laboratory of Ophthalmology, Zhongshan Ophthalmic Center, Sun Yat-Sen University, Guangzhou, China

[b]Hainan Eye Hospital and Key Laboratory of Ophthalmology, Zhongshan Ophthalmic Center, Sun Yat-sen University, Haikou, China

[c]Department of Ophthalmology and Visual Sciences, Washington University School of Medicine, St. Louis, Missouri, United States

[d]Mason Eye Institute, Department of Ophthalmology, University of Missouri School of Medicine, Columbia, MO, United States

Abstract

Purpose: We have demonstrated that deletion of fibroblast growth factor receptor 2 gene (*Fgfr2*) leads to Meibomian gland (MG) atrophy in an inducible conditional knockout mouse model, referred as $Fgfr2^{CKO}$. Herein, we investigated whether MG spontaneously recovers after atrophy in this model.

Methods: Two months old $Fgfr2^{CKO}$ mice were injected peritoneally once or twice of doxycycline (Dox) at 80 μg/gm of body weight to induce MG atrophy of various severities via *Fgfr2* deletion. Recovery of acinar and ductal tissues was monitored by meibography, lipid staining and immunofluorescence against keratin-6a in MG whole-mount. Biomarkers for acinar and ductal differentiation and proliferation were also examined by immunostaining.

Results: Single Dox injection in $Fgfr2^{CKO}$ mice caused severe acinar and moderate ductal atrophy. Severe ductal shortening or loss occurred after second Dox injection, presumably related to the reported slower cycling of the ductal epithelia. Spontaneous acinar regrowth after atrophy

*Corresponding author. State Key Laboratory of Ophthalmology, Zhongshan Ophthalmic Center, Sun Yat-Sen University, Guangzhou, China. zhongxwu@mail.sysu.edu.cn (X. Zhong).

Declaration of competing interest

The authors have no commercial interest in any concept or product discussed in this article.

Appendix A. Supplementary data

Supplementary data to this article can be found online at https://doi.org/10.1016/j.jtos.2021.11.005.

The holocrine secretory unit of MG acinus consists of functional acini being connected by intercalated ductules to the main duct. In the homeostatic MG, the fast cycling meibocytes are sustained by the actively proliferative cells residing in the duct-acinar junctions as previously suggested [11]. We have demonstrated in this report that *Fgfr2* deletion in K14+ epithelial cells of MG results in severe acinar atrophy of MGs. More importantly, spontaneous tissue recovery can occur after MG atrophy in this mouse model. With the increased frequency of Dox injection (Dox-2x), more pronounced damage to the MG ductal system occurs leading to a more protracted MG regenerative process. The regenerating acini appeared to be closely associated with the presence of intercalated ductules (see Figs. 3 and 5). Consistent with prior hypotheses proposed by Jester et al. [11], our results further support the notion that the renewal of acinar and ductal compartments may not be lineage-restricted. The ductal progenitors (black) might give rise to acinar cells (red and yellow) to allow acinar recovery from MG atrophy.

was observed over a period of 60 days in both injection regimens. However, less robust acinar recovery was associated with more disrupted ductal structures in twice injected *Fgfr2*^{CKO} mice.

Conclusions: Our current findings further substantiate the role of FGFR2 in MG homeostasis, and suggest that FGFR2-signaling may provide a potential strategy for regenerating acini from age-related MG dysfunction in humans. Our data demonstrated that spontaneous MG recovery depends on the extent of ductal atrophy, suggesting that ductal epithelia may provide the progenitor cells for acinar regeneration. Nonetheless, the role of ductal tissue as the source of acinar progenitors awaits further investigation.

Keywords

Meibomian gland; Meibomian glands dysfunction; FGFR2; dry eye; Blepharitis; Regeneration; Knockout mouse

1. Introduction

Meibomian glands (MGs) are modified sebaceous glands embedded in the tarsal plate of the eyelid. The main function of MGs is to produce meibum (lipid), which is the main component of the outmost layer of the tear film. Meibum prevents aqueous tears from rapid evaporation, thus stabilizing the tear film and maintaining ocular surface homeostasis [1]. Like the sebaceous glands associated with hair follicles, MGs are holocrine glands. As the lipid-producing meibocytes undergo differentiation to reach maturation, the cells rupture and release meibum to the ductal system, which then delivers the meibum onto the ocular surface via orifice (the opening of the MG duct at the lid margin) [2]. To maintain MG homeostasis, these holocrine glands require continuous replacement of meibocytes in the acini from self-renewal of the basal epithelial cells, which progressively differentiate into mature meibocytes.

Recent epidemiological studies have revealed a high prevalence of dry eye disease (DED) ranging from 4% to 40% worldwide [3]. Among the different forms of DED, Meibomian gland dysfunction (MGD) is the leading cause of evaporative dry eye (EDE) [4]. Patients with MGD develop clinical symptoms with varying degrees of severity, including ocular irritation, foreign body sensation, and visual disturbance. The main treatment options for MGD include oral antibiotics, artificial tears and warm compresses [5]. These treatments transiently relieve the symptoms, but the pathogenesis and effective cure for MGD remain elusive.

MGD is a multifactorial disease and loss of MG homeostasis is a main contributing factor. With recent increased use of non-invasive meibography to examine MGs during clinical examination, it has been shown that gland atrophy and dropouts along with decreased meibum secretion are common features in age-related MGD [6,7]. In addition to aging, other factors, such as sex hormones, ocular inflammation, chemicals, and anti-glaucoma drugs, can also lead to impaired MGs [8]. In other epithelial tissues, such as the skin and intestines with a fast turnover rate, multiple progenitors and stem cell populations are crucial for cell renewal, tissue repair and regeneration [9,10]. It is therefore highly conceivable that MG should have the capability of self-repair and regeneration to maintain its homeostasis. This

hypothesis is supported by the finding that progenitor cells located in the MG ductules are responsible for maintaining the acinar and ductular tissues [11]. However, the prevailing thought regarding reversibility of MG is that MGs do not regenerate once they became atrophic in age-related MGD of humans [12]. Many questions remain to be investigated, such as whether age-related gland atrophy is due to the decline and deficiency of glandular stem/progenitor cells and whether the putative progenitor cells can contribute to MG repair and restore homeostasis following insult or injury.

We previously reported a mouse model in which acinar tissue atrophy can be induced by conditional deletion of *Fgfr2* in MGs [13]. In the current study, a dual-colored reporter mouse line was first generated to validate the inducible Cre recombinase activity in the MGs and in other ocular surface tissues. We then established the MG atrophy model of various severities in the *Fgfr2* mice, and investigated whether spontaneous recovery of MGs can occur after induced atrophy. We found that acinar regeneration is closely associated with the integrity of the residual MG ductal system in this mouse model. Our results further support the notion that progenitor cells derived from the ductal epithelia may play a role in acinar regeneration and glandular recovery.

2. Materials and methods

2.1. Mouse lines

All transgenic mice were bred at the Animal Science Research Center of the University of Missouri (Columbia, MO, USA), in accordance with the institutional guidelines on the Care, Welfare and Treatment of Laboratory Animals. The animal protocol was approved by the University of Missouri Institutional Animal Care and Use Committee (IACUC). All the experiments conformed to the standards in the ARVO Statement for the Use of Animals in Ophthalmic and Vision Research. The triple transgenic mice of *K14rtTA;tetOCre;Fgfr2*$^{fl/fl}$ (referred as *Fgfr2*^{CKO}) were generated as previously described [13]. To generate the Dox-inducible reporter mouse line, *Rosa*^{mTmG} mice were obtained from Jackson Laboratory (JAX stock#007676, Bar Harbor, ME) and bred to the *K14rtTA* (JAX stock#008099) and the *tetOCre* (JAX stock#006224) mice to generate triple transgenic mice *K14rtTA;tetOCre;Rosa*^{mTmG} [21,22]. Genotyping of the transgenic mice was performed on mouse tail DNA, following the conditions and primers recommended for each JAX mouse line listed above.

2.2. Dox administration

Two-month-old reporter mice or *Fgfr2*^{CKO} mice were injected intraperitoneally (i.p.) with doxycycline (Dox) (Sigma-Aldrich, Cat# 324385) dissolved in phosphate buffer saline (PBS) at a dose of 80 μg/gm body weight (B.W.). Dox was given either once (Dox-1x) or twice (Dox-2x), with 7 days between each injection (as illustrated in Fig. 1B), to activate Cre recombinase expression in the Keratin-14 (K14)-expressing epithelial cells.

2.3. In vivo imaging, meibography and oil-red-O (ORO) staining

For in vivo imaging of the MGs, mice were anesthetized with avertin [14] and the upper eyelids were inverted to expose the MGs under Leica M165 FC fluorescence

stereomicroscope to capture meibographs by a CCD camera. After a post-Dox chase, the tarsal plates were dissected from the eyelids for meibographs and then for whole-mount ORO staining to visualize the lipid contents in the MGs. Tissues were placed in 60% 2-propanol for 10 min, stained with ORO solution (Sigma-Aldrich, Cat# O0625) for 15 min, destained with 60% 2-propanol for 1 min, and then mounted on a glass slide for viewing and image capturing under a bright field microscope.

For ORO staining of cryosections, the slides were rinsed with PBS, treated with 60% 2-propanol for 30 s, stained with ORO solution for 15 min, and destained with 60% 2-propanol for 3 min. For LipidTOX (Invitrogen, cat# H34476) fluorescent staining, the stock solution was diluted at 1:200 ratio, sections were stained for 30 min at room temperature, rinsed with PBS, and mounted with Mowiol (Sigma-Aldrich, Cat#10849) for viewing and imaging.

2.4. Histology and immunostaining

Mouse ocular tissues, including eyelids, eye globes, lacrimal glands and Harderian glands, were harvested, fixed in 4% paraformaldehyde overnight, and then processed for either cryosections to examine the expression of EGFP in the reporter mice, or for paraffin sections stained by hematoxylin and eosin (H&E).

Immunofluorescence and immunohistochemistry staining was performed as previously described [13]. Tissue sections were treated with 10 mM of sodium citrate buffer at 95 °C for 10 min for antigen retrieval, followed by incubation in 3% hydrogen peroxide in PBS for 30 min to inactivate endogenous peroxidase activity for immunohistochemistry. Sections were blocked in 5% horse serum in PBST (PBS plus 0.5% Triton X-100) for 1 h and then incubated overnight at 4 °C with primary antibodies against the following antigens: Keratin 6a (K6a) (1:2000; Biolegend); K7 (1:2000; Novusbio); K14 (1:1000; Biolegend); p63 (1:1000; Abcam); PCNA (1:1000; Abcam); and PPAR-γ (1:500, Cell Signaling). After washing with PBS, slides were incubated at room temperature for 1 h with either fluorophore-conjugated or biotinylated secondary antibodies from Thermo-Fisher Scientific (Rockford, IL, USA) and Vector Laboratory (California, USA), respectively. For immunofluorescence, cell nuclei were stained with 4′,6-diamidino-2-phenylindole (DAPI). For immunohistochemistry, color was developed by using an ABC kit from Vector Laboratory and a DAB tablet from Sigma, and counterstained with hematoxylin for cell nuclei.

2.5. Whole-mount immunofluorescence staining

Tarsal plates were fixed in 4% paraformaldehyde for 30 min and rinsed with PBS. Tissue samples were incubated in a blocking solution containing 10% serum in TBST (Tris-buffered saline containing 0.15% Tween-20) overnight at room temperature. Primary antibody against K6a (Biolegend) were diluted at 1:500 in blocking solution and incubated for 24 h on a rocking plate at 4 °C. After washing with PBS, the tarsal plates were incubated in Alexa Fluor 488 conjugated secondary antibody overnight at room temperature. Samples were rinsed with TBST and mounted with Mowiol (Sigma-Aldrich, Cat#10849). Images were acquired using a Leica TCS SP8 MP inverted spectral confocal microscope.

2.6. Statistical analysis

To document the efficiency of acinar recovery in the Dox-injected *Fgfr2*^{CKO} mice, the acini-containing MGs, shown on meibographs, were marked manually and the counts were recorded using NIH Image J software. To calculate the total acinar area, the ORO-stained meibographs were converted into a binary format, the glandular area was outlined manually using the lasso tool and the selected area was measured using the Photoshop CS6 software. Statistical tests were performed using GraphPad Prism 7.0 (GraphPad Software, San Diego, CA). The data were presented as mean ± SEM, and analyzed using unpaired Student's t-tests, with $p < 0.05$ representing statistically significance.

3. Results

3.1. Dox-induced Cre activation and EGFP reporter gene expression in MGs and ocular surface tissues

We previously demonstrated that feeding *Fgfr2*^{CKO} mice ad libitum with Dox-chow can induce *Fgfr2* deletion in the MGs and lead to glandular atrophy [13]. To better control the Dox dosing and visualize the Cre-mediated gene recombination in the MGs, we generated a reporter mouse line (*K14-rtTA;tetO-Cre;Rosa*^{mTmG}) (Fig. 1A), and the dynamics of EGFP expression were examined by pulse-chase experiments (Fig. 1B). The EGFP fluorescence in the inner eyelids of the reporter mice could be displayed by in vivo imaging (Fig. 1C and C1). At the end of chase, cryosections of tarsal plates were prepared to examine the EGFP expression in the MGs (Fig. 1D–F and Fig. S1). After a short chase (1–3 days), EGFP was readily visible in most acini and weakly expressed in the ductal basal layer (Fig. 1D and Figs. S1B–S1C). In the ductal tissues, EGFP fluorescence extended from the basal layer to the suprabasal layers as the chase time progressed (Fig. 1D–E and Fig. S1B–S1D1). When a second (booster) Dox injection was given on day 7, EGFP fluorescence remained longer in the acini (Fig. 1F). When the Dox dosage was increased from 20 to 80 μg/gm body B.W., more EGFP + cells were seen in MGs (Figs. S1B–S1D). Overall, our results indicate that injection of Dox once (referred to Dox-1x) is sufficient to turn on the Cre-mediated gene recombination in the MGs, and a booster injection on day 7 (Dox-2x) can enhance the duration of Cre activity in the acinar tissue.

The Dox-induced EGFP expression has also been demonstrated in other ocular surface tissues where the K14 promoter is active [15]. Strong EGFP fluorescence was seen in the conjunctival epithelium in both Dox-1x and −2x reporter mice (Fig. 1D–F and Fig. S1). In contrast, a single Dox injection at the higher dose (80 μg/gm BW) was insufficient to induce EGFP expression in the corneal epithelium, lacrimal gland or Harderian gland in the reporter mice (data not shown). In the Dox-2x reporter mice, a mosaic EGFP pattern was seen in the corneal epithelium after a 14-day chase (Fig. 1G). In these mice, only a few EGFP-positive cells were detected in the lacrimal and Harderian glands (Fig. 1H and I, respectively). They appeared to be the ductal and myoepithelial cells (indicated by arrowheads and arrows, respectively). Overall, our data substantiate that, by adjusting the dosage and frequency of Dox injection, the Cre activity in the MGs and conjunctival epithelium can be modulated with high efficiency and specificity in this inducible transgenic mouse model.

3.2. Dox-induced Fgfr2 deletion results in both acinar and ductal atrophy in MGs

FGFR2 is expressed in the MG acini, ducts and meibocytes [13]. Two-month-old *Fgfr2*^{CKO} mice were injected with Dox at 80 μg/gm B.W., either once or twice (7 days apart), to induce MG atrophy via *Fgfr2* deletion. When examined on day 14 (Fig. 2B and C), the mutant mice in both groups developed ocular symptoms, including ocular irritations and thickening of the lid margins. The dissected tarsal plates stained with ORO showed severe acinar atrophy in the Dox-injected *Fgfr2*^{CKO} mice (Fig. 2E–F), a result consistent with our previous finding that FGFR2 is required to maintain MG homeostasis in adult mice [13].

The MG ductal system was examined in the *Fgfr2*^{CKO} mice by immunostaining with a ductal biomarker [16], keratin-6a (K6a), on the transverse sections of the upper eyelids after a 14-day chase (Fig. 2G–I). Compared with the controls, ductal cell loss was found in both Dox-injected groups, but was more severe in the Dox-2x group. To demonstrate the intercalated ductular structure in the control mice (arrows in Fig. 2G), K6a immunofluorescence was co-localized with LipidTOX (a fluorescent lipid dye). This ductular structure was found to be attenuated in the Dox-1x and mostly depleted in the Dox-2x *Fgfr2*^{CKO} mice (Fig. 2H–I). These findings suggest that Fgfr2 -deletion induced by a higher dose of Dox resulted in both acinar and ductal atrophy.

To better illustrate the intricate relationship between MG acini and ductal systems, transillumination meibographs, followed by immunofluorescent staining of whole-mount with anti-K6a, were performed on the tarsal plates from the upper eyelids (Fig. 3A–3C1). Our results showed that, compared with the control mice, the MG main ducts were thinner in both groups of *Fgfr2*^{CKO} mice after Dox-injection. Severe ductal tissue atrophy, including depletion of the ductules and shortening of the main ducts, was seen in the Dox-2x mice. This result confirms that, while simultaneous atrophy of acinar and ductal tissues occurred in the Dox-injected *Fgfr2*^{CKO} mice, a more pronounced obliteration of the ductal structure was noted in the Dox-2x mice.

3.3. Spontaneous MG recovery following Dox-induced atrophy

Progressive acinar regeneration after Dox-induced atrophy in both groups of *Fgfr2*^{CKO} mouse (n = 3 in each group) was monitored consecutively for 14, 30, and 60 days by in vivo imaging (Fig. 4A–D). To compare the MG recovery between the two Dox-injected groups with different severities of ductal atrophy, tarsal plates were dissected after 30-day chase, stained with ORO (Fig. 4E–G) and then prepared for cryosections (Fig. 4E1–4G1). Compared with the respective OROstaining patterns on day 14 (Fig. 2D–F), evident acinar regeneration was noted in both groups. However, the acini were more robust and uniformly distributed across the tarsal plate in the Dox-1x *Fgfr2*^{CKO} mice (Fig. 4F). In contrast, the acini varied greatly in size in association with glandular shortening and dropouts (indicated by arrows and asterisks in Fig. 4G, respectively) in the Dox-2x *Fgfr2*^{CKO} mice. Cryosections showed that the recovered glands in Dox-1 mice were structurally normal but smaller, when compared with the controls (Fig. 4E1–4F1). In contrast, the MGs in Dox-2x mice displayed a high degree of heterogeneity in glandular size, and most of the MGs were structurally abnormal, with the absence of acini and ductules associated with the main ducts (Fig. 4G1). To quantify the efficiency of acinar recovery, we quantified the number of

acini-containing MGs and calculated the total acinicontaining area in the controls, Dox-1x, and Dox-2x mice (Fig. 4H–J). At the end of the 30- and 60-day chases, more MGs and a larger total acini-containing area were observed in the Dox-1x than in the Dox-2x mice (p_{30d} = 0.0062 and p_{60d} = 0.0158 for acini-containing MGs; p_{30d} = 0.0175 and p_{60d} = 0.0059 for total acini-containing area). Taken together, these results suggest that MG recovery spontaneously occurred after induced MG atrophy in both groups of mice, but the recovery was compromised with severe ductal atrophy in the Dox-2x mice.

The spontaneous recovery was chased for 60 and 120 days in the Dox-2x mice to examine glandular remodeling by meibography in conjunction with whole-mount K6a immunofluorescence (Fig. 5). Total gland dropout was noted in a lower eyelid after a prolonged (120 days) chase (Fig. 5B1). When cryosections were prepared from the K6a-labeled whole mount and co-stained with LipidTOX, the intercalated ductular structures extending into the adjacent acinus (indicated by large arrows in Fig. 5A2–5B2) were missing in the acini-free glands (small arrows in Fig. 5A2), suggesting that it is highly likely that the intercalated ductule is intricately related to the acinar regeneration.

3.4. Expression of biomarkers in the recovered MGs

We investigated whether induced *Fgfr2* deletion caused a prolonged suppression of cell proliferation in the MGs by immunofluorescence of PCNA-K14 co-staining (Fig. 6A–C1). In normal MGs, PCNA + cells were found in the ductal and acinar basal epithelial layer (arrows in Fig. 6A). This expression pattern was also seen in the recovered MGs in both groups of Dox-injected mice (Fig. 6B–C). Interestingly, PCNA was strongly expressed in the basal epithelium of the duct that associated with minimal or no acinar tissue (Fig. 6C1), suggesting that compromised acinar regeneration in the Dox-2x mice was not due to the suppression of cell proliferation.

In addition to K6a, the expression of K7 (another ductal marker) was examined in the MGs (Fig. 6D–F1). The inner ductal structures appeared similar between the control and the Dox-1x mice (Fig. 6D–E), but abnormal ductal structures containing a high density of K7+ cells were noted in the Dox-2x mice (Fig. 6F–F1). Lipid synthesis markers of meibocytes, including PPAR-γ (a transcription factor) and fatty acid synthase (FASN), were examined (Fig. S2). Similar to the normal MGs, these lipid-synthesis markers were expressed in the regenerated acini. However, whether meibocyte maturation is impaired in the Dox-2x mice awaits further investigation.

The transcription factor, p63, is considered as a progenitor and stem cell marker in many epithelial tissues [17,18]. In normal MGs, p63-positive cells were found in the acinar and ductal basal epithelial layers (Fig. 6G). This expression pattern was also seen in the MGs of the Dox-1x mice after a 60-day chase (data not shown). In the MGs of the Dox-2x mice, p63 was expressed in the basal layer of ducts associated with or without adjacent acini (Fig. 6H–H2), suggesting that the progenitor cells committed to acinar regeneration were deficient after the second Dox-injection.

4. Discussions

Meibomian gland atrophy and glandular dropouts are prominent clinical features of aged-related MGD [7]. However, current understanding of MG homeostasis and regeneration remains limited. Herein, we demonstrate a spontaneous recovery of murine MGs after significant acinar loss and ductal atrophy induced by conditional deletion of *Fgfr2* in a mouse model. Our findings suggest that the efficiency and extent of glandular restoration are highly dependent on the integrity of the MG ductal system. The surviving MG ductular network appears to modulate the capacity of acinar regeneration after induced MG atrophy. The overall scheme of the MG regrowth after MG atrophy induced by depletion of *Fgfr2* observed from this study is depicted in Fig. 7.

Exploiting our previously reported $Fgfr2^{CKO}$ mice, we further induced an animal model with either moderate or severe MG atrophy via single or repetitive induction in the present study. Intraperitoneal injection of Dox efficiently activated the Cre recombinase in both reporter mice (Fig. 1) and $Fgfr2^{CKO}$ mice (Fig. 2). In our previous report [13], even though we have demonstrated compromised acinar proliferation with MG atrophy after conditional deletion of *Fgfr2* in MGs, we did not observe consistent ductal degeneration, presumably due to the inconsistent oral intake or gastrointestinal (GI) uptake of Dox chow by the transgenic mice associated with the disruption of GI epithelia due to the *Fgfr2* deletion. Upon intraperitoneal injection of Dox in the current study, $Fgfr2^{CKO}$ mice manifested consistent Cre recombinase expression (Fig. 1) and tunable extents of MG acinar loss, thinning of ductal epithelia, ductular degeneration and glandular dropouts (Fig. 2). While mice with twice Dox injections had more severe phenotypes than those with single injection, in Fig. 2, all mice were harvested at day 14. Thus, those mice with only single injection may have additional one week to recover from the *Fgfr2* deletion by Dox. Nevertheless, the MG atrophy impacted by these differences in timing should be less critical for longer chase periods as shown in Figs. 4 and 5. The ductal tissues appears more resistant than the acinar tissues in response to *Fgfr2* loss (Fig. 3), possibly due to a relatively slower turnover rate in the ductal epithelial cells compared with that in acinar cells [19]. Progressive loss of FGFR2 signaling via a booster of Dox injection may potentially further decrease the surviving ductal cells of MGs (Fig. 3). Our data suggest that FGFR2 is essential for maintaining the structural integrity of both acinar and ductal tissue of MGs.

The deletion of *Fgfr2* in MG leads to notable ductular atrophy and the inability of the remaining ductal tissues (Fig. 3), suggesting an essential role of FGFR2 signaling in maintaining branched ductal structures of MG. In postnatal development, FGFR2 signaling has been suggested to regulate the survival and/or proliferation of basal cells during ductal branching and acinar generation in numerous tissues [20–22]. Consistent with a previous report in K5-Fgfr2-null mice [23], striking sebaceous gland atrophy, concomitant with the meibomian gland atrophy, was also observed in our study (data not shown). And similarly, conditional knockout of *Fgfr2* in branching exocrine organs–including the lacrimal glands, salivary glands, lung and mammary glands, also leads to compromised ductal branching and failure of glandular regeneration [24–28]. These data suggest that deletion of *Fgfr2* impairs proliferation and directional migration of the ductal basal cells, therefore hampering the ductal to acinar differentiation process under normal and injured conditions [29]. Thus, our

data implies that the level of FGFR2 expression in MG is highly relevant to survival and eventual regrowth for both acinar and ductal epithelial cells of MG.

In the present study, we report for first the time that murine MG is capable of self-restoration after glandular atrophy (Figs. 4 and 5). Similar to the normal MGs, the regenerated acini after induced atrophy were still capable of expressing normal differentiation markers such as FASN and PPARγ [Fig. S2] [25], along with abundant production of lipid contents, as evidenced by the strong staining with oil red O (Fig. 4), indicating they were functionally active meibocytes. The robust restoration of MG following moderate glandular loss is likely mediated through an active self-renewal process. However, severe MG ductal atrophy may not be reversible, implying the existence of a limited capacity for ductular and associated acinar self-regeneration. Interestingly, in Dox-2x group, we observed the regenerating MGs displayed robust thickened ductal epithelium but without restoration of connected ductule and regenerating acini (Fig. 5). We surmise that the progenitor cells destined for acinar lineage was deficient or compromised after induced atrophy.

Another provoking finding of this study is that the acinar replenishment after MG atrophy is highly dependent on the remaining ductules (Figs. 3 and 5). Based on the essential role of FGFR2 in branching morphogenesis and recovery found in other epithelial tissues, such as the lung and salivary gland [30,31], the ductal lineages of MG might serve as an important progenitor pool responsible for glandular restoration. Type II (basic) Keratin 5 (K5) which heterodimerizes with type I (acidic) Keratin 14 (K14) to form the intermediate filaments that constitute cytoskeleton, is widely expressed in mouse and human MGs [13,16]. As described in a previous label-retaining study in the homeostatic MGs, the quiescent $K5^+$ progenitors responsible for MG renewal are localized in the terminal end of the Keratin 6 $(K6)^+$ ductal epithelium [11]. The authors further postulated two hypotheses regarding the MG turnover and progenitors - A: the ductal and acinar epithelia is individually maintained by the $K5^+/K6^+$ and $K5^+/K6^-$ unipotent label-retaining cells (LRCs), respectively; or B: the ductal and acinar epithelia are commonly maintained by the $K5^+$ bipotent LRCs which subsequently evolve into $K5^+/K6^+$ and $K5^+/K6^-$ LRCs [11]. In the Dox-2x group, we found that ductal cells appeared to be robustly regenerated in some recovering ducts while acini were notably absent (Fig. 5). The uneven regeneration between the acinar and ductal cells suggests that the ductal/ductular differentiation and related ductular/-acinar differentiation during the early stage of recovery were impeded after severe glandular atrophy. Thus, our finding is more in line with hypothesis B than A, because one stem cell (SC) or progenitor cell differentiates into ductule and then ductule into acinus (Fig. 7). Furthermore, our data on the inverse correlation between ductal atrophy and acinar regeneration after *Fgfr2* deletion suggests that FGFR2 is crucial for the renewal of both types of progenitor cells. Nevertheless, the exact lineage of MG progenitors contributing to ductal and acinar recovery awaits further investigations.

In our current empirical model of MG regeneration after atrophy, it remains possible that MG regeneration can arise from cells with less or no deletion of *Fgfr2* due to a dose-dependent difference in deletion efficiency between the Dox-1x and Dox-2x mice. However, as the *Fgfr2* is extensively expressed in MG acinar and ductal tissues, the amount of surviving MG cells expressing *Fgfr2* could be inversely correlated with the extent of

physical disruption to the MG ductal tissues. An alternative possibility is that the MG regeneration may be activated from those more primitive MG cells which are less affected by loss of FGFs or do not express *Fgfr2*. Further investigations are required for identification of those cells specifically responsible for the dynamic process of MG regeneration.

In clinical studies, evidence on whether atrophic MGs in aged population can regrow or not remains inconclusive, due to various confounding factors associated with patients' pre-existing skin or lid conditions and diverse treatment modalities [32–35]. Reversal of MG dropouts and increase of MG area have been reported following various treatments for MGD associated with ductal obstruction or MG hypertrophy [32,36–38]. However, definitive reversal of atrophic MGs has never been reported. In addition, other studies showed that treatments for MGD can improve symptoms but no change on MG atrophy [35,39]. Nowadays, quantitative analysis of meibographic images has been more widely used to assess the MG structure and glandular area in MGD patients [40,41]. Although this method is more objective and reproducible than the meiboscore, both methods quantify primarily the activity of lipid-producing acini, but not the surrounding ductal structures. Our findings in the $Fgfr2^{CKO}$ mouse model suggest that acinar regrowth after atrophy is predicated by the ductal structure with regenerative potential. Extrapolating our empirical findings to humans, clinical modalities to preserve or regenerate the ductal system potentially should improve the lipid-producing acinar activity. Nonetheless, current clinical reports on obstructed MGD indicate that the ocular immuno-inflammatory involvement is highly relevant to MGD severity [42–44]. However, ocular inflammation was not readily detected in our mouse model and it may be partially due to the use of Dox injection to induce MG atrophy via deletion of *Fgfr2*, as doxycycline can exert anti-inflammatory effects on ocular surface and is often used clinically for treating MGD. Furthermore, a recent animal study showed that inhibition of ceramide synthesis ameliorates the SCD1 deficiency-induced abnormal meibum secretion and MG atrophy, suggesting that local lipid microenvironment plays an essential role in the pathogenesis of MGD and has therapeutic potential for obstructive MGD [45]. Whether adverse immune and lipid microenvironment would directly impact MG ductal epithelial cells during glandular restoration in our mouse model and MGD patients awaits further investigations and is beyond the scope of this current report.

As demonstrated in our previous report using $Fgfr2^{CKO}$ mice, the FGF/FGFR signaling pathways are crucial in MG homeostasis. In the current report, we further substantiate the role of FGF/FGFR2 in glandular regeneration. Our dose-dependent *Fgfr2* deletion system can reproducibly induce severe acinar atrophy in MG with spontaneous and efficient glandular recovery. Our study may pave the way for future exploration of MG regeneration after age-mediated MG atrophy or dysfunctions. Furthermore, it is known that aging is a major risk factor for MGD with glandular atrophy [46]. The process of aging is associated with impairment of tissue repair, such as decline of stem/progenitor cells and/or increase of cell senescence. We intend to exploit the current animal model in future studies to evaluate age-related changes in MG recovery by administering Dox to induce MG atrophy of various severities at different ages to delineate the regenerating process. Delineating the underlying pathogenesis and the related regeneration mechanism should provide a new therapeutic paradigm to optimize the clinical management of MGD via direct restoration of the MGs.

There are limitations to the present study. The promising biomarkers for MG acinar and ductal progenitor cells are not currently known. Therefore, we have yet to address how FGFR2 signaling contribute to MG recovery at a cellular level [26,28,43]. Further lineage-labeled studies using diverse lineage-specific promotors would be beneficial for elucidating the underlying molecular and cellular mechanisms steering MG restoration.

5. Conclusions

We have demonstrated in the triple transgenic mice (*K14rtTA; tetOCre, Rosa*^{mTmG}) that Cre activity and EGFP reporter gene expression in the MGs can be modulated by the Dox dosage and administering frequency. Using this inducible system, a MG atrophy model with tunable severities was established and the essential role of FGFR2 in MG homeostasis was further substantiated in this study [13]. More importantly, the current study further supports the notion that the MG ductal structure plays a critical role in spontaneous glandular recovery and acinar regeneration after induced atrophy. Overall, we have provided a valuable animal model for future exploration of the therapeutic potentials of FGFR2-signaling for MG regeneration and for investigation on the MG progenitor/stem cells in these processes.

Supplementary Material

Refer to Web version on PubMed Central for supplementary material.

Funding

This work was supported by NEI grant EY029106 (to LWR and AJWH) from the National Institutes of Health, the Open Research Funds of the State Key Laboratory of Ophthalmology (2017KF04) and Hainan Province Clinical Medical Center.

Abbreviations

MGs	Meibomian glands
FGFR2	fibroblast growth factor receptor 2
MGD	Meibomian glands dysfunction
DED	dry eye disease

References

[1]. Bron AJ, et al. Functional aspects of the tear film lipid layer. Exp Eye Res 2004;78 (3):347–60. [PubMed: 15106912]

[2]. Knop E, et al. The international workshop on meibomian gland dysfunction: report of the subcommittee on anatomy, physiology, and pathophysiology of the meibomian gland. Invest Ophthalmol Vis Sci 2011;52(4):1938–78. [PubMed: 21450915]

[3]. Stapleton F, et al. TFOS DEWS II epidemiology report. Ocul Surf 2017;15(3):334–65. [PubMed: 28736337]

[4]. Craig JP, et al. TFOS DEWS II definition and classification report. Ocul Surf 2017;15(3):276–83. [PubMed: 28736335]

[5]. Sabeti S, et al. Management of meibomian gland dysfunction: a review. Surv Ophthalmol 2020;65(2):205–17. [PubMed: 31494111]

[6]. Arita R, et al. Noncontact infrared meibography to document age-related changes of the meibomian glands in a normal population. Ophthalmology 2008;115(5):911–5. [PubMed: 18452765]

[7]. Den S, et al. Association between meibomian gland changes and aging, sex, or tear function. Cornea 2006;25(6):651–5. [PubMed: 17077655]

[8]. Schaumberg DA, et al. The international workshop on meibomian gland dysfunction: report of the subcommittee on the epidemiology of, and associated risk factors for, MGD. Invest Ophthalmol Vis Sci 2011;52(4):1994–2005. [PubMed: 21450917]

[9]. Gonzales KAU, Fuchs E. Skin and its regenerative powers: an alliance between stem cells and their niche. Dev Cell 2017;43(4):387–401. [PubMed: 29161590]

[10]. van der Flier LG, Clevers H. Stem cells, self-renewal, and differentiation in the intestinal epithelium. Annu Rev Physiol 2009;71:241–60. [PubMed: 18808327]

[11]. Parfitt GJ, et al. Renewal of the holocrine meibomian glands by label-retaining, unipotent epithelial progenitors. Stell Cell Rep. 2016;7(3):399–410.

[12]. Jones L, et al. TFOS DEWS II management and therapy report. Ocul Surf 2017;15 (3):575–628. [PubMed: 28736343]

[13]. Reneker LW, et al. Fibroblast growth factor receptor 2 (FGFR2) is required for meibomian gland homeostasis in the adult mouse. Invest Ophthalmol Vis Sci 2017;58(5):2638–46. [PubMed: 28510629]

[14]. Weiss J, Zimmermann F. Tribromoethanol (Avertin) as an anaesthetic in mice. Lab Anim 1999;33(2):192–3. [PubMed: 10780824]

[15]. Mouse strain datasheet-004782, The Jackson Laboratory.

[16]. Parfitt GJ, et al. Absence of ductal hyper-keratinization in mouse age-related meibomian gland dysfunction (ARMGD). Aging 2013;5(11):825–34. [PubMed: 24259272]

[17]. Senoo M, et al. p63 Is essential for the proliferative potential of stem cells in stratified epithelia. Cell 2007;129(3):523–36. [PubMed: 17482546]

[18]. Pellegrini G, et al. p63 identifies keratinocyte stem cells. Proc Natl Acad Sci U S A 2001;98(6):3156–61. [PubMed: 11248048]

[19]. Olami Y, et al. Turnover and migration of meibomian gland cells in rats' eyelids. Ophthalmic Res 2001;33(3):170–5. [PubMed: 11340409]

[20]. Arman E, et al. Fgfr2 is required for limb outgrowth and lung-branching morphogenesis. Proc Natl Acad Sci U S A 1999;96(21):11895–9. [PubMed: 10518547]

[21]. Pond AC, et al. Fibroblast growth factor receptor signaling is essential for normal mammary gland development and stem cell function. Stem Cell 2013;31(1):178–89.

[22]. De Moerlooze L, et al. An important role for the IIIb isoform of fibroblast growth factor receptor 2 (FGFR2) in mesenchymal-epithelial signalling during mouse organogenesis. Development 2000;127(3):483–92. [PubMed: 10631169]

[23]. Grose R, et al. The role of fibroblast growth factor receptor 2b in skin homeostasis and cancer development. EMBO J 2007;26(5):1268–78. [PubMed: 17304214]

[24]. Chatzeli L, Gaete M, Tucker AS. Fgf10 and Sox9 are essential for the establishment of distal progenitor cells during mouse salivary gland development. Development 2017;144(12):2294–305. [PubMed: 28506998]

[25]. Balasooriya GI, et al. FGFR2 is required for airway basal cell self-renewal and terminal differentiation. Development 2017;144(9):1600–6. [PubMed: 28348168]

[26]. Yuan T, et al. FGF10-FGFR2B signaling generates basal cells and drives alveolar epithelial regeneration by Bronchial epithelial stem cells after lung injury. Stell Cell Rep. 2019;12(5):1041–55.

[27]. Parsa S, et al. Terminal end bud maintenance in mammary gland is dependent upon FGFR2b signaling. Dev Biol 2008;317(1):121–31. [PubMed: 18381212]

[28]. Thotakura S, Basova L, Makarenkova HP. FGF gradient controls Boundary position between proliferating and differentiating cells and regulates lacrimal gland growth dynamics. Front Genet 2019;10:362. [PubMed: 31191595]

[29]. Zhang X, et al. FGF ligands of the postnatal mammary stroma regulate distinct aspects of epithelial morphogenesis. Development 2014;141(17):3352–62. [PubMed: 25078648]

[30]. May AJ, et al. Diverse progenitor cells preserve salivary gland ductal architecture after radiation-induced damage. Development 2018;145(21).

[31]. Liu Q, et al. Lung regeneration by multipotent stem cells residing at the bronchioalveolar-duct junction. Nat Genet 2019;51(4):728–38. [PubMed: 30778223]

[32]. Yin Y, Gong L. Reversibility of gland dropout and significance of eyelid hygiene treatment in meibomian gland dysfunction. Cornea 2017;36(3):332–7. [PubMed: 27755193]

[33]. Guillon M, Maissa C, Wong S. Eyelid margin modification associated with eyelid hygiene in anterior blepharitis and meibomian gland dysfunction. Eye Contact Lens 2012;38(5):319–25. [PubMed: 22890229]

[34]. Finis D, et al. Six-month effects of a thermodynamic treatment for MGD and implications of meibomian gland atrophy. Cornea 2014;33(12):1265–70. [PubMed: 25321941]

[35]. Bilkhu PS, Naroo SA, Wolffsohn JS. Randomised masked clinical trial of the MGDRx EyeBag for the treatment of meibomian gland dysfunction-related evaporative dry eye. Br J Ophthalmol 2014;98(12):1707–11. [PubMed: 24997178]

[36]. Arita R, et al. Topical diquafosol for patients with obstructive meibomian gland dysfunction. Br J Ophthalmol 2013;97(6):725–9. [PubMed: 23584719]

[37]. Maskin SL, Testa WR. Growth of meibomian gland tissue after intraductal meibomian gland probing in patients with obstructive meibomian gland dysfunction. Br J Ophthalmol 2018;102(1):59–68. [PubMed: 28592418]

[38]. Hura AS, et al. Visible meibomian gland structure increases after vectored thermal pulsation treatment in dry eye disease patients with meibomian gland dysfunction. Clin Ophthalmol 2020;14:4287–96. [PubMed: 33324034]

[39]. Aronowicz JD, et al. Short term oral minocycline treatment of meibomianitis. Br J Ophthalmol 2006;90(7):856–60. [PubMed: 16613920]

[40]. Koprowski R, et al. A quantitative method for assessing the quality of meibomian glands. Comput Biol Med 2016;75:130–8. [PubMed: 27286185]

[41]. Xiao P, et al. An automated and multiparametric algorithm for objective analysis of meibography images. Quant Imag Med Surg 2021;11(4):1586–99.

[42]. Reyes NJ, et al. Neutrophils cause obstruction of eyelid sebaceous glands in inflammatory eye disease in mice. Sci Transl Med 2018;10(451).

[43]. Singh PP, et al. Meibomian gland dysfunction is suppressed via selective inhibition of immune responses by topical LFA-1/ICAM antagonism with lifitegrast in the allergic eye disease (AED) model. Ocul Surf 2021;21:271–8. [PubMed: 33812087]

[44]. Mahajan A, et al. Aggregated neutrophil extracellular traps occlude Meibomian glands during ocular surface inflammation. Ocul Surf 2021;20:1–12. [PubMed: 33401018]

[45]. Ji C, et al. Inhibition of ceramide de novo synthesis ameliorates meibomian gland dysfunction induced by SCD1 deficiency. Ocul Surf 2021;22:230–41. [PubMed: 34474170]

[46]. Wolffsohn JS, et al. Demographic and lifestyle risk factors of dry eye disease subtypes: a cross-sectional study. Ocul Surf 2021;21:58–63. [PubMed: 33965652]

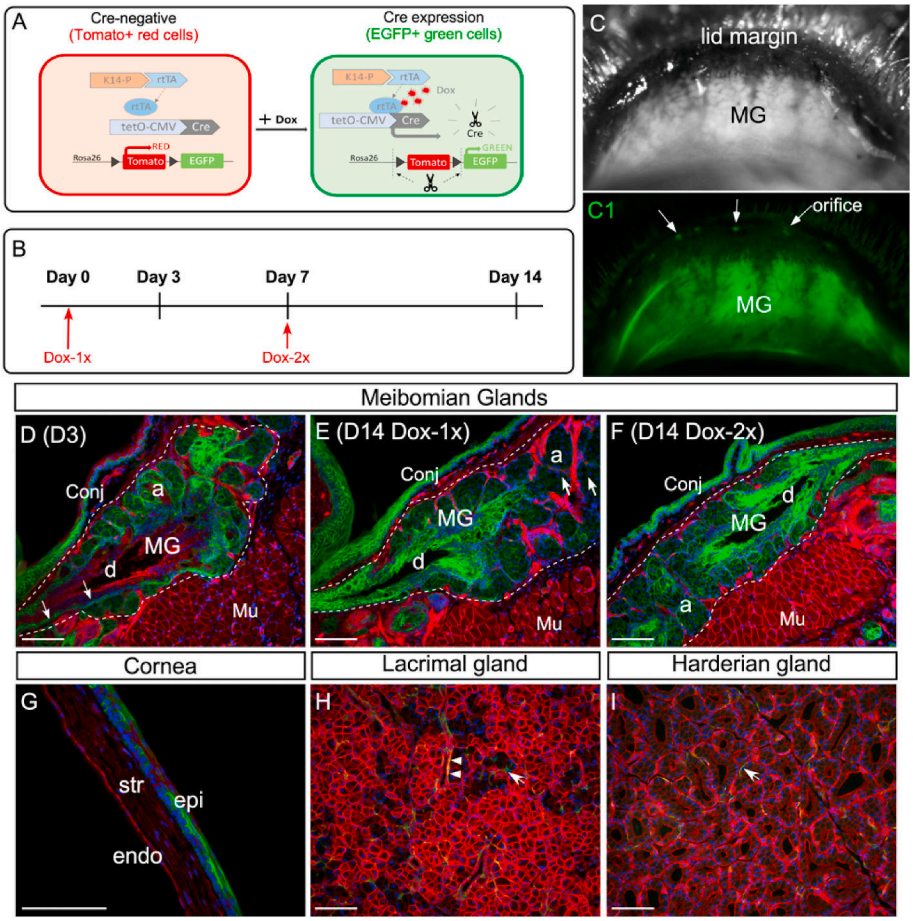

Fig. 1.

Dox-induced EGFP expression in the ocular surface tissues and glands of the reporter mice. (A) Illustration of the dual fluorescence reporter system in the triple transgenic mice (*K14rtTA;tetOCre; Rosa*^{mTmG}). In the absence of Dox, all cells express Tomato (red) fluorescence. Upon Dox induction, Cre recombinase is activated by reverse tetracycline-controlled transactivator (rtTA) driven by the K14 promoter, resulting in the expression of EGFP (green fluorescence) in the K14-positive cells. (B) Experimental scheme. (C and C1) Live imaging of MGs in a reporter mouse after 14-day chase from the first Dox injection. The MGs were shown under regular (C) and fluorescent (C1) illumination. Arrows point to the MG orifice. (D–E) Cryosections of upper eyelids from Dox-injected reporter mice stained with nuclear dye DAPI (blue). The MG area was outlined by dotted line. On day 3 (D3) after the first injection, EGFP fluorescence was readily seen in the acini (a) and was weakly visible in the basal epithelium of the central duct (d) (indicated by arrows in D). After 14-day chase, EGFP fluorescence was diminished in some acini (arrows in E) as a result of the holocrine secretion process in MGs. In the central duct, EGFP expression was expanded from the basal to the suprabasal layers during the chase from D3 (D) to D14 (E). EGFP was also expressed in the conjunctival epithelium (conj) as early as D3. (F) When two sequential doses of Dox was given on D1 and D7 (Dox-2x, as illustrated in B), EGFP fluorescence was present in most of the acini on D14. (G) Mosaic EGFP expression in the corneal epithelium on D14 in the Dox-2x reporter mice. (H–I) Weak EGFP expression in

the lacrimal gland (H) and Harderian gland (I) after 14-day chase. A few EGFP-positive myoepithelial cells (arrows in H and I) and ductal cells (arrowheads in H) were identified in these glands. Abbreviations: a, acini; d, duct; MG, meibomian gland; conj, conjunctiva; epi: corneal epithelium; str: stroma; endo: corneal endothelium; Mu: Muscle. Scale bar in each figure represents 100 μm.

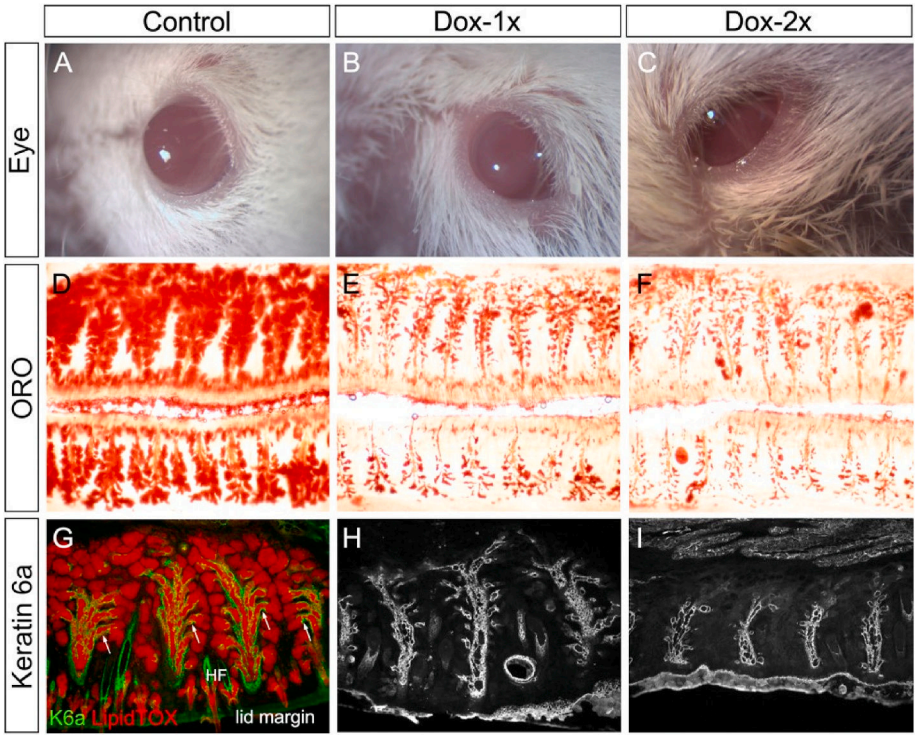

Fig. 2.

MG atrophy induced by Dox injection in the *Fgfr2*^{CKO} mice. (A–C) Eye appearance on D14. Compared to the control mice (A), the lid margin became thickened in the Dox-injected *Fgfr2*^{CKO} mice (B, C). Eyelids were partially closed and lid margins were irregular in the Dox-2x *Fgfr2*^{CKO} mice (C). (D–F) Tarsal plates dissected from upper and lower eyelids stained with lipid dye ORO. Abundant lipid-producing acini were shown in control mice (D). Severe acinar atrophy in both Dox-1x (E) and Dox-2x (F) *Fgfr2*^{CKO} mice on D14. (G–I) Colocalization of K6a immunofluorescence (red) and LipidTOX (green) on transverse sections of upper eyelids in control MGs (G). K6a immunofluorescence showed ductal atrophy in both Dox-injected groups of *Fgfr2*^{CKO} mice (H and I) on D14, but more severe in the Dox-2x mice than in the Dox-1x mice (compare H to I).

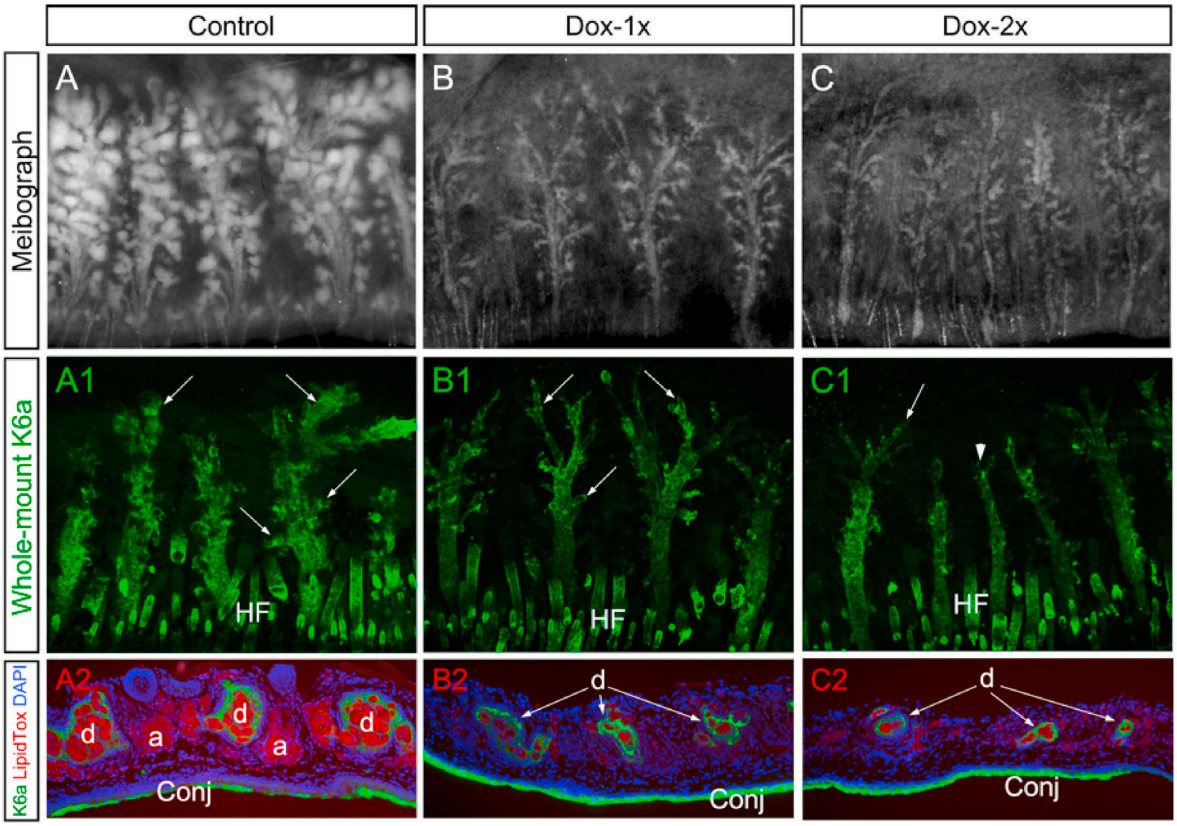

Fig. 3.

MG acinar and ductal atrophy shown respectively by meibography and whole-mount K6a immunofluorescence staining of tarsal plates. (A–C) Meibographs showed normal (A) and atrophic acini in Dox-1x (B) and Dox-2x (C) *Fgfr2*^{CKO} mice on D14 after the first Dox-injection. (A1-C1) Corresponding to the meibographs shown in A-C, whole-mount K6a immunofluorescence (green) of tarsal plates exhibited progressive loss and atrophy of the ductal tissues in the Dox-injected *Fgfr2*^{CKO} mice (B1 and C1) when compared with the control (A1). The ductal branches (arrows) were either attenuated (B1 and C1) or completely lost in the distal end of the MGs (arrowhead in C1) in the Dox-injected *Fgfr2*^{CKO} mice. (A2-C2) The whole-mount K6a-stained tarsal plates were processed for cryosections and co-stained with LipidTOX (red) to further demonstrate both acinar and ductal atrophy in the Dox-injected *Fgfr2*^{CKO} mice, which occurred more severely in the Dox-2x than in the Dox-1x mice. Abbreviation: HF, hair follicle.

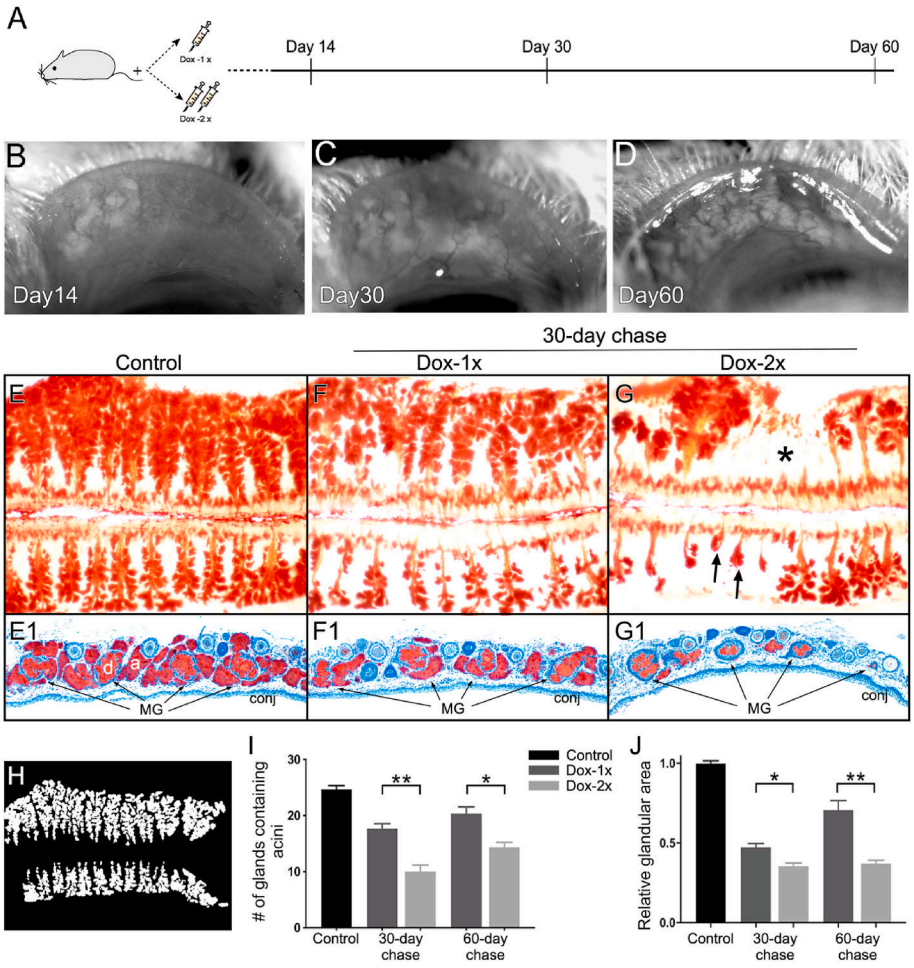

Fig. 4.

Spontaneous glandular recovery after Dox-induced atrophy in *Fgfr2*^{CKO} mice. (A) Experimental scheme to examine MG recovery from atrophy. (B–D) *In vivo* imaging showing severe MG atrophy on D14 (B) followed by progressive acinar regeneration on D30 (C) and D60 (D) in a Dox-1x *Fgfr2*^{CKO} mouse. (E–G) ORO whole mount staining of paired eyelids in the control (E), Dox-1x (F) and Dox-2x (G) *Fgfr2*^{CKO} mice after 30-day chase. Gland dropout (asterisk in G) and shortening (arrows in G) were noted in the Dox-2x mouse. (E1-G1) Cryosections of the corresponding ORO-stained tarsal plates counter-stained with hematoxylin to confirm the different degree of glandular recovery from atrophy in the Dox-1x and Dox-2x mice. (H–J) Quantitative analysis of MG acinar tissue recovery. The ORO-stained meibographs were converted into the binary images for quantitative analysis (H). The number of MGs containing lipid-producing acini (I) and the total recovered glandular area (J) were calculated. Reduced acinar recovery was associated with more severe ductal damage in the Dox-2x *Fgfr2*^{CKO} mice. Data was shown as mean ± SEM. n = 3 mice per group, *$p < 0.05$, and **$p < 0.01$.

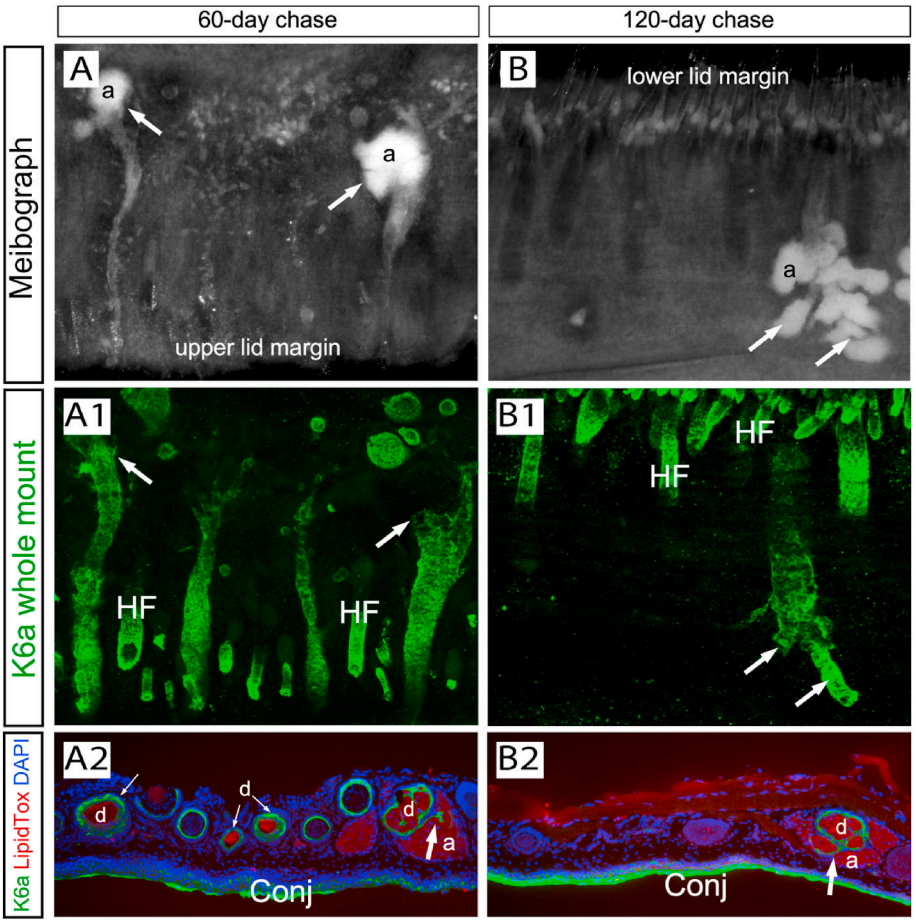

Fig. 5.

Extended chase to examine MG recovery in Dox-2x *Fgfr2*^{CKO} mice. (A-A2) After 60-day chase, meibography showed active regeneration of acini (a) in the distal area (arrows in A), which corresponded to the robust ductal structures shown by the K6a whole-mount immunofluorescence (arrows in A1). The K6a-stained tarsal plates were processed for cryosections and stained with LipidTOX (red) to demonstrate the intercalated ductular structure (large arrow in A2) connecting the acini and the main duct (d). (B–B2) After 120-day chase, persistent glandular dropout was seen in some areas of the lower eyelid of the Dox-2x group (B1 and B2). Acinar regeneration was closely associated with the ductal branch structures (indicated by arrows in B and B1). The intercalated ductule was pointed by the arrow in B2. .

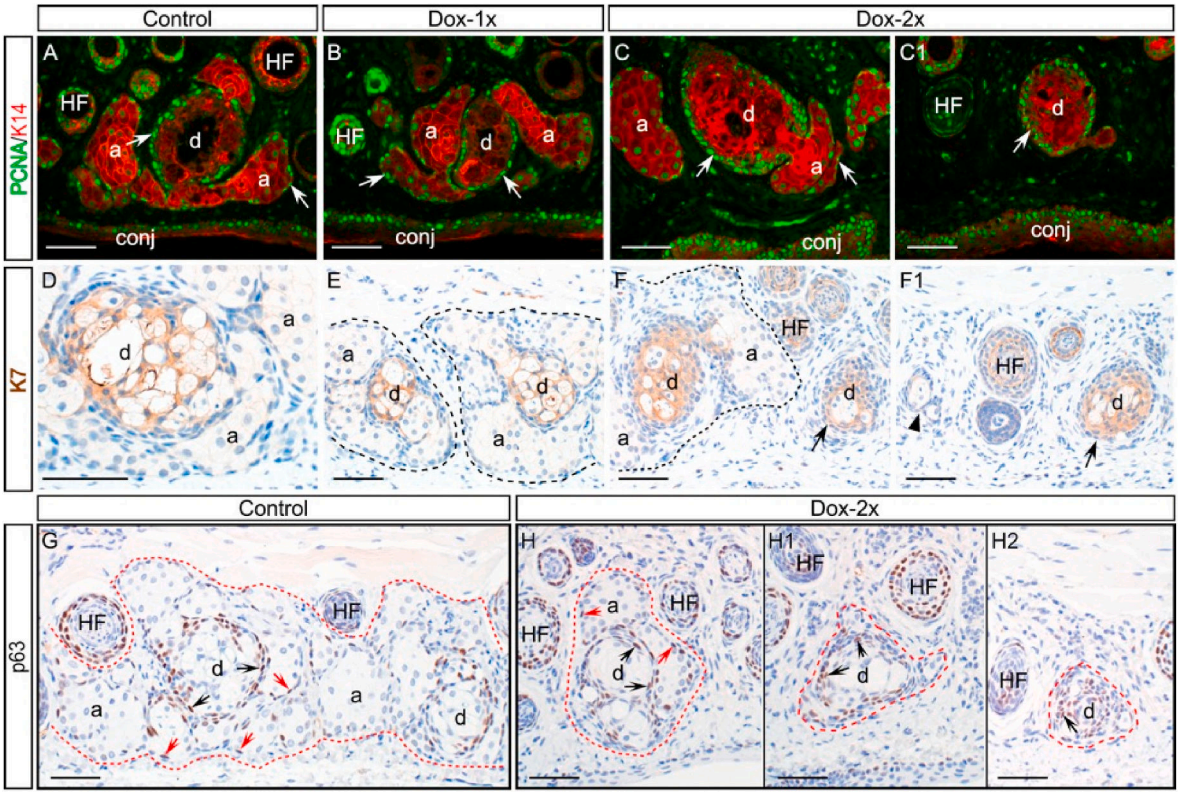

Fig. 6.

Expression of biomarkers in the Dox-injected *Fgfr2*^{CKO} mice after 60-day chase. (A-C1) Colocalization of PCNA (green) and K14 (red) immunofluorescence. In control mice (A), PCNA was expressed in the basal epithelium of the MG acini and ducts (indicated by arrows). Similar pattern was seen in the MGs of the Dox-1x *Fgfr2*^{CKO} mice (B). In the Dox-2x mice, PCNA was strongly expressed in the basal layer of the ducts associated either with or without acini (arrows in C and C1, respectively). (D-F1) Expression of ductal marker K7 in the MGs by immunohistochemistry. The ductal structures appeared normal in the Dox-1x *Fgfr2*^{CKO} mice (E) when compared with the control (D). In the Dox-2x mice, while K7 was expressed in the MG ducts, the ductal cells appeared less differentiated, particularly in the areas with severe acinar atrophy (arrows in F and F1). The MG acinar area was outline by dotted line. A residual MG was indicated by arrowhead in F1. (G-H2) p63 Immunohistochemistry. In control mice (G), p63 was mostly expressed in the ductal basal layer (indicated by black arrows), and only a few p63+ cells were found in the acinar compartment (indicated by red arrows). Similar pattern was seen in the recovered MG of Dox-2x *Fgfr2*^{CKO} mice (H). Despite of the heterogeneous MG ducts in the Dox-2x mice, p63 expression was present in the ductal epithelia associated with or without adjacent acini (indicated by black arrows in H–H2). .

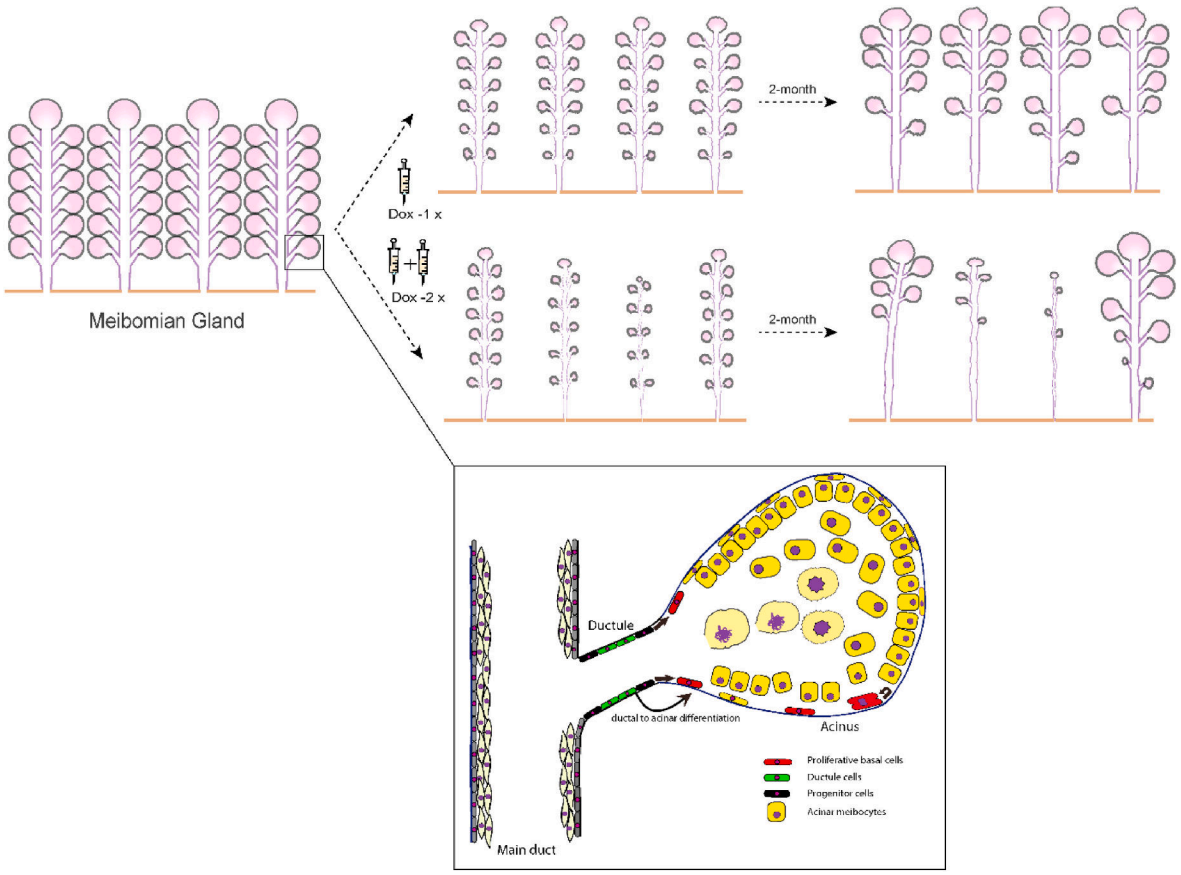

Fig. 7.

Schematic illustration of spontaneous MG repair and regeneration after inducible MG atrophy in *Fgfr2*^{CKO} mice.